Mixed Finite-Element Method for Composite Cylinder Subjected to Impact

William E. Bachrach*
Columbia University, New York, New York
and
R. Scott Hansen†
Spaulding Fibre, Smyrna, Tennessee

The Hellinger-Reissner variational principle in the time domain is used to formulate a frame-invariant hexahedral element in the natural coordinate system that exhibits high coarse-mesh accuracy for problems involving bending. A modified Hertzian contact law for a sphere on a cylinder is utilized to compute the contact force on the cylinder. The Tsai-Wu failure criterion is used to determine if failure has occurred in the element of the impact region. The element development, low-velocity impact computation, and failure criterion are implemented in an explicit time integration scheme. Results are given for three problems that are used in verifying the time integration code and to view the failure propagation in the impact region of the cylinder.

I. Introduction

FOR low-velocity impact, the damage of a composite cylinder may not be visible until catastrophic failure is about to occur. Some examples of low-velocity impact problems, could be an instrument that has dropped on the cylinder during manufacturing, a forklift colliding with the cylinder, and foreign objects or projectiles impacting on the surface of a cylinder. In all of these examples, the question "Does sequential failure exist?" becomes very important in determining if the impact damage is significant. Sequential failure is the hierarchy between matrix cracking, delamination, and fiber breakage. The impact damage may be insignificant if the energy-absorbing phenomenon is dominant: matrix cracking and/or delamination. However, if fiber breakage occurs during impact damage, then catastrophic failure could become a reality. Rather than determining the mechanisms for failure, this paper examines how the failure propagates in the impact region of the composite cylinder during low-velocity impact, if the strength and mechanical moduli of the composite material do not change.

A mixed variational principle is used to formulate three-dimensional hexahedral elements to model the composite cylinder experiencing impact damage. For static equilibrium at the element level, potential energy is minimized, and only the displacement field can be chosen. Unfortunately, there are many applications for which these C^0 isoparametric plane, axisymmetric, and three-dimensional elements do not approximate very well the exact solution for pure bending, pure shear, and incompressibility problems using a coarse mesh. To overcome this difficulty, variational principles have been developed so that the displacement, strain, and stress fields can be chosen independently; i.e., the Hu-Washizu variational principle allows all three fields to be chosen, whereas the Hellinger-Reissner variational principle allows only the displacement and the stress fields to be chosen. A discussion of the development of plane and three-dimensional elements using variational principles and the rationale for the elements selected are discussed by Pian,[1] Herrmann,[2] Mandell et al.,[3] Wang et al.,[4] Pian and Sumihara,[5] Belytschko and Bachrach,[6] and Bachrach.[7] In structural dynamics, the strain-displacement governing equations are relaxed in the Hamilton functional using a Lagrange multiplier technique, and the procedure for developing the linear system of equations of the finite-element method is essentially the Hu-Washizu variational principle in the time domain. For this case, the interest is in capturing the pure bending phenomena of the cylinder; thus, a lower-order polynomial is used in approximating the shear stress, with the linear elastic stress-strain law being exactly satisfied.

A modified Hertzian contact law is used in describing the geometrical and deformational relationship between the impact of the sphere and the composite cylinder. The contact force of the sphere on the composite cylinder is computed using force-deformation and indentation laws for loading and unloading cycles in conjunction with an iterative method to solve the nonlinear contact force equation.[8-13]

For a lumped (diagonal) mass matrix, the linear system of second-order differential equations can be decoupled using the central-difference explicit time integration scheme. When the equations are decoupled, storage of the global stiffness matrix and equation-solving routines are not necessary. At multiple time steps, the stresses are computed in the impact region, and the Tsai-Wu failure criterion is used to determine if damage has occurred. This criterion can only designate that failure has occurred, and it is not intended to explain the mechanisms of failure.

Lee[14,15] and Lee et al.[16] have presented three-dimensional finite-element and dynamic analysis for damage accumulation in the composite and composite laminates subjected to impact which are pertinent to this work.

In the next section, a mixed variational element is developed by choosing independent displacement and stress fields using the Hellinger-Reissner variational principle in the time domain, so that the element can better approximate pure bending. Section III presents the low-velocity impact computation, and the Tsai-Wu failure criterion is discussed in Sec. IV. The three ingredients are then implemented into an explicit time integration algorithm in Sec. V. Section VI presents three examples, with the first two examples verifying the explicit time integration and low-velocity impact computation code, and the last example determining the failure propagation in the impact region of the composite cylinder.

II. Element Development

The three-dimensional hexahedral element is developed using the Hellinger-Reissner variational principle (HR) in the

Received Aug. 10, 1987; revision received Feb. 8, 1988.

*Assistant Professor, Department of Civil Engineering and Engineering Mechanics. Member AIAA.
†Advanced Composite Development Engineer.

time domain. This variational principle is composed of the potential energy functional, kinetic energy, and a relaxed strain-displacement governing equation, with the stress-strain equation exactly satisfied. For a single element, this functional can be written as

$$\Pi_{HR}(\boldsymbol{u},\boldsymbol{\sigma}) = \int_t \Pi_{PE} - T_{KE} - \int_\Omega \boldsymbol{\sigma}^T(\boldsymbol{D}^{-1}\boldsymbol{\sigma} - \nabla^s\boldsymbol{u})\,\mathrm{d}\Omega\,\mathrm{d}t \quad (1)$$

where Π_{PE} is the potential energy functional, T_{KE} the kinetic energy functional, $\boldsymbol{u}$ the displacement field, $\boldsymbol{\sigma}$ the stress field, $\boldsymbol{D}$ the matrix of material properties (for a composite laminate this matrix includes the ply orientation of the lamina), ∇^s the symmetric part of the displacement gradient, and the superscript T designates the transpose of a matrix. The potential energy functional, the kinetic energy, the stresses, and the symmetric part of the displacement gradient are

$$\Pi_{PE} = \frac{1}{2}\int_\Omega \boldsymbol{\sigma}^{\mathrm{T}}\boldsymbol{D}^{-1}\boldsymbol{\sigma}\,\mathrm{d}\Omega - \sum_{I=1}^{8} \boldsymbol{d}_I^T\boldsymbol{f}_I \quad (2a)$$

$$T_{KE} = \frac{1}{2}\int_\Omega \rho\boldsymbol{u}\ddot{\boldsymbol{u}}\,\mathrm{d}\Omega \quad (2b)$$

$$\boldsymbol{\sigma}^T = [\sigma_x,\ \sigma_y,\ \sigma_z,\ \sigma_{xy},\ \sigma_{yz},\ \sigma_{zx}] \quad (2c)$$

$$\nabla^s\boldsymbol{u}^T = [u_{x,x},\ u_{y,y},\ u_{z,z},\ u_{x,y} + u_{y,x},\ u_{y,z} + u_{z,y},\ u_{z,x} + u_{x,z}] \quad (2d)$$

where $\boldsymbol{d}_I^T = (d_{xI}, d_{yI}, d_{zI})$ are the displacements at node I, $\boldsymbol{f}_I^T = (f_{xI}, f_{yI}, f_{zI})$ are the nodal forces at node I, ρ is the density of the material, a comma in the subscript denotes partial differentiation, and the superscript dot denotes the time derivatives.

The weak form corresponding to the stationary point of the Π_{HR} functional is

$$\delta\Pi_{HR}(\boldsymbol{u},\boldsymbol{\sigma}) = \int_t\int_\Omega [\rho\delta\boldsymbol{u}^T\ddot{\boldsymbol{u}} - \delta^T(\boldsymbol{D}^{-1}\boldsymbol{\sigma} - \nabla^s\boldsymbol{u}) + \delta\nabla^s\boldsymbol{u}^T\boldsymbol{\sigma}]\,\mathrm{d}\Omega - \sum_{I=1}^{8}\delta\boldsymbol{d}_I^T\boldsymbol{f}_I\,\mathrm{d}t = 0 \quad (3)$$

where $\boldsymbol{u}$ must be a C^0 function, whereas $\boldsymbol{\sigma}$ may be a piecewise continuous C^{-1} function with discontinuities.

The standard C^0 isoparametric interpolation for the eight-node hexahedral element is

$$\boldsymbol{u}(\xi,\eta,\zeta) = \sum_{I=1}^{8}\boldsymbol{d}_I N_I \quad (4a)$$

$$N_I = \tfrac{1}{8}(1 + \xi_I\xi)(1 + \eta_I\eta)(1 + \zeta_I\zeta) \quad (4b)$$

where ξ_I, η_I, and ζ_I are the coordinates of node I in the reference plane.

The symmetric part of the displacement gradient is

$$\nabla^s\boldsymbol{u} = \begin{Bmatrix} u_{x,x} \\ u_{y,y} \\ u_{z,z} \\ u_{x,y} + u_{y,x} \\ u_{y,z} + u_{z,y} \\ u_{z,x} + u_{x,z} \end{Bmatrix} = \boldsymbol{Bd} \quad (5)$$

The stress field is separated into constant c, bending b, and shear s components:

$$\boldsymbol{\sigma} = [\boldsymbol{S}_c,\ \boldsymbol{S}_b,\ \boldsymbol{S}_s]\boldsymbol{s} = \boldsymbol{Ss} \quad (6a)$$

where

$$\boldsymbol{s}^T = [s_1,\ s_2 \cdots s_{18}] \quad (6b)$$

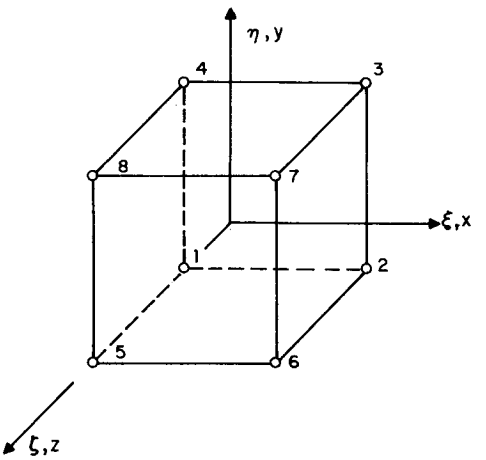

Fig. 1 Physical and reference plane representation of the hexahedral element.

$$\boldsymbol{S}_c = \boldsymbol{I}_{(6\times 6)} \quad (6c)$$

$$\boldsymbol{S}_b = \begin{bmatrix} \eta & 0 & 0 & 0 & \zeta & 0 & \eta\zeta & 0 & 0 \\ 0 & 0 & \xi & 0 & 0 & \zeta & 0 & \zeta\xi & 0 \\ 0 & \eta & 0 & \xi & 0 & 0 & 0 & 0 & \xi\eta \\ & & & & \boldsymbol{0}_{(3\times 9)} & & & & \end{bmatrix} \quad (6d)$$

$$\boldsymbol{S}_s = \begin{bmatrix} & & & \boldsymbol{0}_{(3\times 3)} & & \\ 0 & 0 & \zeta & & & \\ 0 & \xi & 0 & & & \\ \eta & 0 & 0 & & & \end{bmatrix} \quad (6e)$$

The stress interpolants in Eqs. (6c–6e) are described in a local coordinate system with the physical and reference planes parallel to each other, as shown in Fig. 1. These interpolants are composed of linear and bilinear polynomials in the natural coordinate system, with some of the shear stress interpolants removed to enhance the accuracy in bending problems using an optimum number of stress parameters; the shear stress is constant in one plane but linear in the direction perpendicular to this plane.[7,17] For skewed two-dimensional meshes, the plane element strain and stress fields developed in the natural coordinate system (ξ,η,ζ) were found to be less sensitive to geometric distortion than their counterpart interpolants defined in the physical plane.[18] Unfortunately, most elements developed by changing the normal and shear stress fields are not frame invariant. This problem is overcome by transforming the stress fields in the reference plane to the physical plane by

$$\sigma_{ij}^{\mathrm{phy}}(x,y,z) = J_k^i J_i^j \sigma_{kl}(\xi,\eta,\zeta) = J_k^i J_i^j \boldsymbol{Ss} = \boldsymbol{S}^*\boldsymbol{s} \quad (7)$$

where J is the Jacobian matrix and S^* the frame invariant interpolants. The Jacobian matrices are computed using one-point integration.[5,19]

For a frame invariant element, the element mass and stiffness matrices are developed by substituting Eqs. (5–7) into Eq. (6). The variation of the Hellinger-Reissner functional becomes

$$\delta\Pi_{HR} = \int_t \delta\boldsymbol{d}^T(\boldsymbol{M}\ddot{\boldsymbol{d}} + \bar{\boldsymbol{B}}^T\boldsymbol{s}) - \delta\boldsymbol{s}^T(\bar{\boldsymbol{D}}\boldsymbol{s} - \bar{\boldsymbol{B}}\boldsymbol{d}) - \sum_{I=1}^{8}\delta\boldsymbol{d}_I^T\boldsymbol{f}_I\,\mathrm{d}t = 0 \quad (8a)$$

where

$$\boldsymbol{M} = \int_\Omega \rho N^T N\,\mathrm{d}\Omega \quad (8b)$$

$$\bar{B} = \int_\Omega S^{*T} B \, d\Omega \tag{8c}$$

$$\bar{D} = \int_\Omega S^{*T} D^{-1} S^* \, d\Omega \tag{8d}$$

The stationary conditions are

$$\bar{D}s = \bar{B}d \tag{9a}$$

$$M\ddot{d} + \bar{B}^T s = f \tag{9b}$$

The stress field σ and the element stiffness K are

$$\sigma = S^* \bar{D}^{-1} \bar{B} d \tag{10a}$$

$$K = \bar{B}^T \bar{D}^{-1} \bar{B} \tag{10b}$$

The element stiffness is a function of the displacement and the stress fields. An efficient formulation of the element stiffness is presented by Bachrach et al.[18] and Bachrach[7] in conjunction with the γ-projection operator[20,21] for plane elements designed in the natural coordinate system or three-dimensional elements designed in the physical plane.

In the time domain, the semidiscretized equations of motion are

$$M\ddot{d} + Kd = f \tag{11}$$

III. Low-Velocity Impact Computation

The Hertzian contact law is a theory of local indentation of two colliding bodies which leads to an equation for the unknown contact force. This law is based on the geometrical relationship between the contact indentation and the deflection of the colliding bodies. For this application, the indentation is a function of the sphere impacting on a cylinder,[22] and the contact force computation is composed of the interaction between the Force-Deformation Law and the Indentation Law. These laws have been used and modified by Sun and Huang,[8] Sun,[9] Tan and Sun,[10] Wu and Chang,[11] and Wu and Springer[12,13] to model the impact of a sphere on a variety of composite beams and plates.

The Force-Deformation Law is the static compression of two isotropic elastic bodies whose surfaces are assumed to be smooth. Along the surface of the bodies the shear stresses must vanish, and the normal stresses acting on the sphere and the cylinder must balance in the contact area. The Force-Deformation Law at time $N+1$ is

$$F^{N+1} = k_1 (\alpha^{N+1})^{1.5} \tag{12}$$

when $0 \le \alpha \le \alpha_M$, where F is the impact force, k_1 a function of the impact and cylindrical geometry, α the indentation of the cylinder due to the sphere, and α_M the maximum indentation corresponding to the maximum contact force. The constant k_1 is

$$k_1 = \frac{4}{3C_E}\left[\frac{1}{\sqrt{(1/R_{\text{sph}}) + (1/2R_{\text{cyl}})}}\right] \tag{13a}$$

$$C_E = \frac{1-\nu^2}{E_{\text{sph}}} + \frac{1}{E_{\text{cyl}}} \tag{13b}$$

where the subscripts sph and cyl are abbreviations for the sphere and cylinder, R is the radius, ν Poisson's ratio, E_{sph} Young's modulus of the sphere, and, for a composite material, E_{cyl} the transverse modulus normal to the fiber direction of the uppermost composite layer. Note that the term $1/E_{\text{cyl}}$ in Eq. (13b) is different from the original Hertzian contact law.

The indentation law is the difference between the displacement of the sphere and the cylinder parallel to the contact force at the next time step:

$$\alpha^{N+1} = w_{\text{sph}}^{N+1} - w_{\text{cyl}}^{N+1} \tag{14}$$

The displacement of the sphere is approximated using the Wilson θ method[23] and Newton's Second Law of Motion:

$$w_{\text{sph}}^{N+1} = w_{\text{sph}}^N + \Delta t \dot{w}_{\text{sph}}^N - (\Delta t^2/6M_{\text{sph}})\,[F^{N+1} + 2F^N] \tag{15}$$

where M_{sph} is the mass of the sphere.

The displacement of the cylinder is approximated using a forward finite-difference approximation:

$$w_{\text{cyl}}^{N+1} = w_{\text{cyl}}^N + \Delta t \dot{w}_{\text{cyl}}^N + (\Delta t^2/2)\,\ddot{w}_{\text{cyl}}^N \tag{16}$$

Substituting Eqs. (15) and (16) into Eqs. (12) and (14), the Force-Deformation Law becomes

$$F^{N+1} = k_1\{ w_{\text{sph}}^N + \Delta t \dot{w}_{\text{sph}}^N - (\Delta t^2/6M_{\text{sph}})[F^{N+1} - 2F^N] - w_{\text{cyl}}^N - \Delta t \dot{w}_{\text{cyl}}^N - (\Delta t^2/2)\ddot{w}_{\text{cyl}}^N \}^{1.5} \tag{17}$$

The contact force is computed using an iterative method to solve the nonlinear equation.

The unloading cycle is

$$F^{N+1} = F_M \left(\frac{\alpha^{N+1} - \alpha_0}{\alpha_M - \alpha_0}\right)^{2.5} \tag{18}$$

The permanent indentation α_0 is

$$\alpha_0 = \alpha_M \left(1 - \frac{\alpha_{\text{cr}}}{\alpha_M}\right)^{1/2.5} \quad \text{when } \alpha_M \ge \alpha_{\text{cr}} \tag{19a}$$

$$\alpha_0 = 0 \quad \text{when } \alpha_M < \alpha_{\text{cr}} \tag{19b}$$

where α_{cr} is the critical indentation of the material. Again, the contact force in the unloading cycle is computed using an iterative method.

IV. Failure Criteria

Many different failure criteria could be used in analyzing the ply failures in the composite cylinder, and these criteria are discussed by Hashin,[24,25] and Reddy and Pandey.[26] The latter reference concluded for in-plane loading that all failure criteria derived from the general tensor polynomial form are equivalent. However, for transverse loading, the Tsai-Hill and maximum strain criterion gave locations for failure different from the others. Since this case study is concerned with the question "How does the failure propagate in an ideal model?", the three-dimensional Tsai-Wu failure criteria is used to analyze the ply failure in the composite cylinder:

$$F_{ij}\sigma_i\sigma_j + F_i\sigma_i \le 1 \tag{20}$$

The scalar constants are

$$F_1 = \frac{1}{X_T} - \frac{1}{X_C}, \quad F_2 = \frac{1}{Y_T} - \frac{1}{Y_C}, \quad F_3 = \frac{1}{Z_T} - \frac{1}{Z_C}$$

$$F_{11} = \frac{1}{X_T X_C}, \quad F_{22} = \frac{1}{Y_T Y_C}, \quad F_{33} = \frac{1}{Z_T Z_C}$$

$$F_{44} = \frac{1}{R^2}, \quad F_{55} = \frac{1}{S^2}, \quad F_{66} = \frac{1}{T^2}$$

$$F_{12} = -\frac{1}{2}\frac{1}{\sqrt{X_T X_C Y_C Y_T}}, \quad F_{23} = -\frac{1}{2}\frac{1}{\sqrt{Y_T Y_C Z_C Z_T}}$$

$$F_{13} = -\frac{1}{2}\frac{1}{\sqrt{X_T X_C Z_C Z_T}} \tag{21}$$

where $X_{T/C}$ are the longitudinal tensile and compressive strengths, $Y_{T/C}$ and $Z_{T/C}$ the transverse tensile and compressive strengths, and R, S, and T the shear strengths in the xy, yz, and xz planes, respectively. The constants $F_{4\text{-}6}$ are zero, since the shear strength is the same for both positive and negative shear stress, and it is assumed that there is no interaction between the shear and normal stresses.

Since the stresses in the failure criteria are defined in the material direction (fiber direction), the stresses must be transformed from the physical plane to the material plane.

V. Explicit Time Integration Algorithm

The semidiscretized equations of motion for each element at time step N is

$$\boldsymbol{M}\ddot{\boldsymbol{d}}^N + \boldsymbol{K}\boldsymbol{d}^N = \boldsymbol{f}^N \tag{22}$$

The central-difference time integration schemes for acceleration and velocity with the time step Δt constant are

$$\ddot{\boldsymbol{d}}^N = \frac{\boldsymbol{d}^{N+1} + 2\boldsymbol{d}^N + \boldsymbol{d}^{N-1}}{\Delta t} \tag{23a}$$

$$\dot{\boldsymbol{d}}^{N+1/2} = \frac{\boldsymbol{d}^{N+1} - \boldsymbol{d}^N}{\Delta t} \tag{23b}$$

The displacements are obtained by substituting Eq. (23a) into Eq. (22):

$$\boldsymbol{d}^{N+1} = \Delta t^2\, \boldsymbol{M}^{-1}(\boldsymbol{f}^N - \boldsymbol{K}\boldsymbol{d}^N) + 2\boldsymbol{d}^N - \boldsymbol{d}^{N-1} \tag{24}$$

The new displacements are computed without solving any system of linear equations. The continuous mass matrix is approximated as a lumped mass matrix

$$M_{IJ} = \frac{\delta_{IJ}}{8}\rho \int_\Omega \mathrm{d}\Omega \tag{25}$$

where δ is the Kronecker delta function.

The explicit time integration scheme is only conditionally stable, and the stability limits the time step in linear systems to

$$\Delta t \le (2/\lambda_{\max}) = \Delta t_{\text{stab}} \tag{26}$$

where $\lambda_{\max}$ is the maximum eigenvalue of the system. The maximum eigenvalue of the system is bounded by the maximum eigenvalue of the element, $\lambda_{\max} \le \lambda^e_{\max}$.

The implementation of this explicit time integration algorithm for this application is presented in Table 1.

Table 1 Explicit time integration algorithm

Assume that the time step for the cylinder has already been computed.

1) At time = 0.0, set the initial conditions:
$$\boldsymbol{d}^0, \dot{\boldsymbol{d}}^{1/2},\ N = 0$$
2) Update the displacements:
$$\boldsymbol{d}^{N+1} = \Delta t\, \dot{\boldsymbol{d}}^{N+1/2} + \boldsymbol{d}^N$$
3) Compute the internal forces of the model by looping through all of the elements in the mesh. The development shown below is not computationally efficient, the element stiffness being computed and assembled at time step $N = 0$. A more efficient algorithm is to implement a pattern recognition procedure for the elements in the model; only the different element stiffnesses in the model are computed during the first time step, and only the upper half of these matrices are stored. Depending on the application, the stresses are computed at a time-step multiple (NMULT*Δt) in the impact region to check for failure within that element.

   Loop through the number of elements.

   a) For time step $N = 0$:
      i) Assemble and store $\bar{\boldsymbol{B}}$ and $\bar{\boldsymbol{D}}^{-1}$.
      ii) Store the upper half of the stiffness matrix:
      $$\boldsymbol{K} = \bar{\boldsymbol{B}}^T \bar{\boldsymbol{D}}^{-1} \bar{\boldsymbol{B}}$$
      iii) Compute the internal force at $N + 1$:
      $$\boldsymbol{f}^{\text{int},N+1} = \boldsymbol{K}\boldsymbol{d}^{N+1}$$
   b) For $N > 0$ and $N \ne N\text{MULT}^*\Delta t$, where NMULT is defined by the user, the internal force is computed using the above equation.
   c) For $N = N\text{MULT}^*\Delta t$, the stresses in the impact region are computed.

   Loop through the number of Gaussian integration points.

      i) Compute the stress at each Gauss point (ξ_G, η_G, and ζ_G) of $\sigma(x,y,z) = \boldsymbol{S}^*(\xi_G, \eta_G, \zeta_G)\, \bar{\boldsymbol{D}}^{-1}\bar{\boldsymbol{B}}\boldsymbol{d}^N$
      ii) Check if failure has occurred by substituting these stress values into the Tsai-Wu failure criterion. In this paper, only the initial failure occurring in the region of impact will be analyzed, and the failure propagation will be determined.
4) Compute the external forces $\boldsymbol{f}^{N+1}$ for loading or unloading using the modified Hertzian contact law outlined in Sec. III.
5) Solve for the accelerations:
$$\ddot{\boldsymbol{d}}^{N+1} = \boldsymbol{M}^{-1}(\boldsymbol{f}^{N+1} - \boldsymbol{K}\boldsymbol{d}^{N+1})$$
6) $N \leftarrow N + 1$.
7) Update the velocities:
$$\dot{\boldsymbol{d}}^{N+1/2} = \Delta t \ddot{\boldsymbol{d}}^N \dot{\boldsymbol{d}}^{N-1/2}$$
8) Go to step 2.

VI. Examples

Three examples are presented: 1) steel sphere impacting on a steel clamped plate (Karas[27]), 2) steel sphere impacting on a graphite-epoxy clamped and simply supported plate (Sun and Chen,[28] Wu,[29] and Wu and Chang[11]), and 3) steel sphere impacting on a CFRP HIM6 epoxy cylinder (Lloyd and Knight[30]).

The first two examples are used to check if the explicit time integration and low-velocity impact algorithms are implemented correctly. The last example determines the failure propagation in the impact region of the composite cylinder. All three examples use the contact force vs time plot as the checkpoint for evaluation; the impactor is a steel sphere modeled as a rigid body, and the computer program is executed on a Cray-XMP/48.

Steel Sphere Impacting on a Steel Clamped Plate

The characteristics of the plate are length is 7.874 in., width is 7.874 in., thickness is 0.315 in., Young's modulus is 30.0 E + 06 psi, Poisson's ratio is 0.30, and density is 0.282 lbm/in.^{3}.

One quadrant of the clamped plate is modeled with four elements in the x, y, and z directions, as shown in Fig. 2. The plate is clamped at the edges $x = y = 0$, and the other two edges are constrained to represent symmetry about $x = y = 3.937$ in. The steel sphere impacts at the center of the clamped plate as a point load with a velocity of 39.37 in./s and a radius of 0.3937 in.

The contact force vs time plot is shown in Fig. 3. The amplitude and the phase of this curve are similar to the results obtained by Wu and Chang.[11] They used a different element (an eight-node isoparametric hexahedral element with incompatible modes) and an implicit time integration scheme. For a static, point-loaded, clamped-plate problem, the mixed variational element used here and the eight-node isoparametric hexahedral incompatible element compute very accurately the displacement at the center of the clamped plate.

Steel Sphere Impacting on a Graphite-Epoxy Clamped Plate

The plate is a 10-plied $[0/90/0/90/0\ \text{deg}]_s$ laminate, and the characteristics of the plate are length is 7.874 in., width is

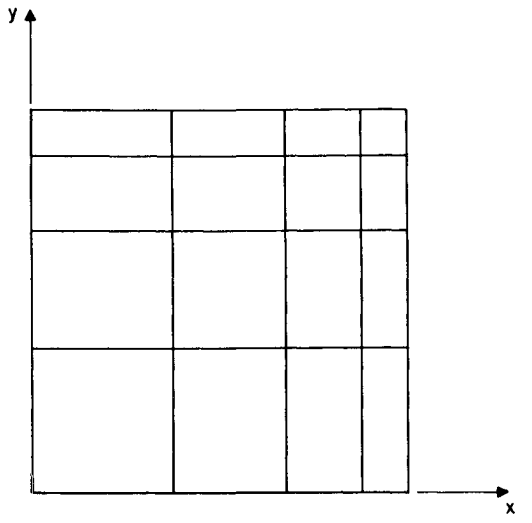

Fig. 2 The nonuniform mesh of one quadrant of the clamped plate.

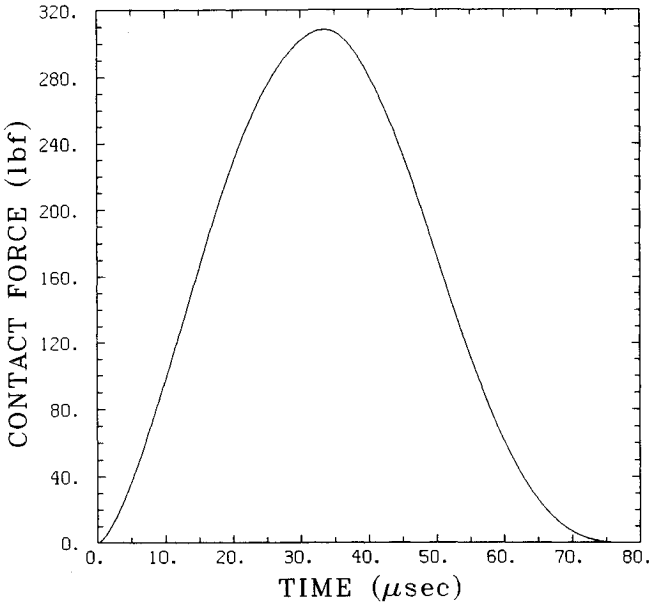

Fig. 3 Contact force for a steel sphere impacting on a steel clamped plate.

7.874 in., thickness is 0.106 in., E_1(fiber modulus) is 17.5 $E + 06$ psi, E_2 (transverse modulus) is 1.15 $E + 06$ psi, ν_{12} is 0.30, ν_{23} is 0.30, $G_{12} = G_{23} = G_{31}$ is 0.80 $E + 06$ psi, density is 0.0571 lbm/in.^{3}, and critical indentation (α_{cr}) is 0.00316 in. The same mesh used in the first example is used here, except that each ply group is modeled with one layer of three-dimensional elements. The steel sphere impacts at the center of the clamped plate as a point load with a velocity of 118.0 in./s and a radius of 0.25 in.

The contact force vs time curve for both boundary conditions is shown in Fig. 4. The maximum contact force and the duration of impact for the simply supported plate are approximately 15 and 33% larger than the results by Chen and Sun.[28] However, as in the previous example, the contact force profile force checked almost exactly with the results obtained by Wu,[29] except that by using the explicit time integration scheme a less filtered profile was computed.

The maximum contact force for both the clamped and simply supported plate problems is very similar, but the phase of the unloading cycle for the simply supported plate is longer. This is attributed to the simply supported plate being more flexible. For both types of boundary conditions, failure propagation in the layers of the composite plate during the loading

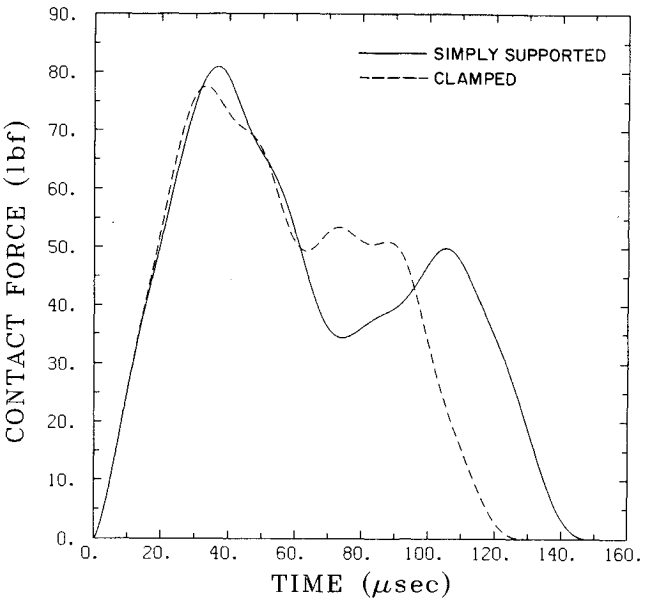

Fig. 4 Contact force for a steel sphere impacting on a graphite-epoxy plate.

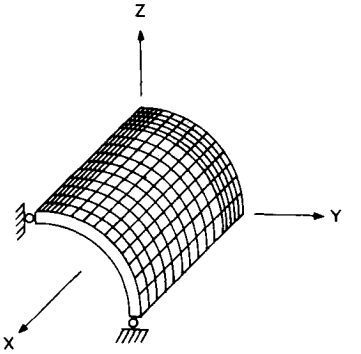

Fig. 5 The nonuniform mesh of the quarter-cylinder's outer hoop layer.

cycle will be very similar. Similar results were obtained by Wu and Chang.[11]

Steel Sphere Impacting on a CFRP HIM6 Epoxy Cylinder

The cylinder is a five-plied external hoop design [$X, X, 0_4$] laminate, and each ply group is modeled with one layer of three-dimensional elements: X = polar layer, and 0 = hoop layer. The 5.75-in.-diam composite cylinder has a cylindrical membrane length-to-diameter ratio of 0.70, and the cylindrical thickness ranges from 0.070–0.080 in. The nonuniform mesh of the outer hoop layer of the quarter-cylinder is shown in Fig. 5. The thickness is exaggerated, and symmetry conditions are applied along all of the edges except at the edge perpendicular to the yz plane and located at x = cylindrical membrane length.

The material characteristics of CFRP HIM6 epoxy for the cylinder are E_1 (fiber modulus) is 29.4 $E + 06$ psi, E_2 (transverse modulus) is 1.624 $E + 06$ psi, ν_{12} is 0.32, ν_{23} is 0.32, $G_{12} = G_{23} = G_{31}$ is 1.22 $E + 06$ psi, density is 0.0578 lbm/in.^{3}, critical indentation (α_{cr}) is 0.00316 in., longitudinal tensile and compressive strength is 507.6/223.4 $E + 03$ psi, transverse tensile and compressive strength is 8.122/21.76 $E + 03$ psi, and shear strength is 14.21 $E + 03$ psi.

For this example, the indentor is modified to be a sphere. The radius stays the same, but the velocity is adjusted so that a shorter duration of impact and a larger maximum contact force are obtained. The steel sphere impacts at the center of the cylinder as a point load with a velocity of 1506.0 in./s and a radius of 0.25 in.

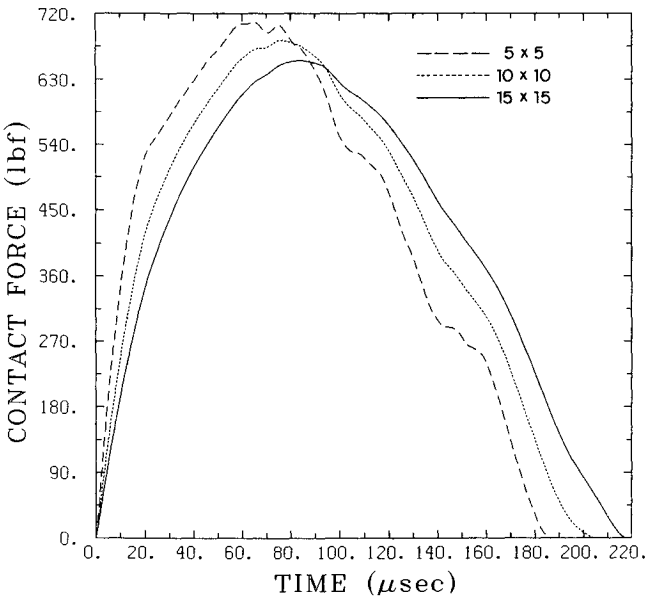

Fig. 6 Contact force of the steel sphere impacting on a CFRP HIM6 epoxy cylinder.

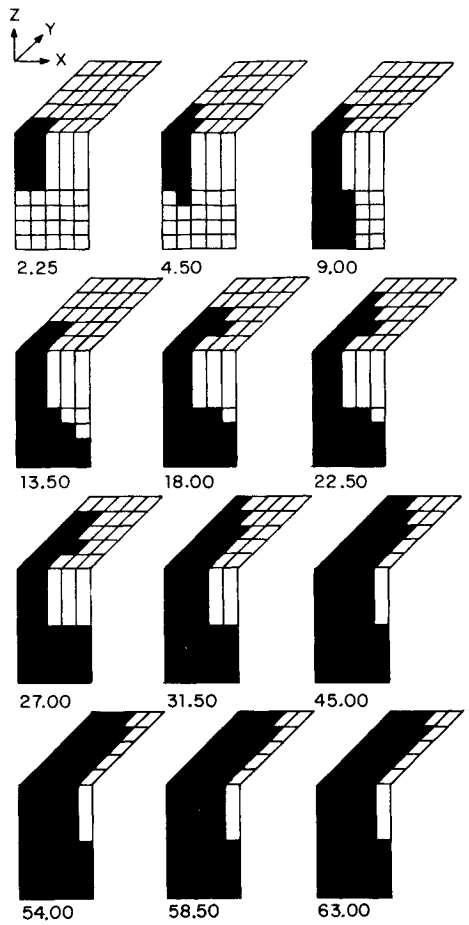

Fig. 7 Failure propagation in the outer hoop layer and along the thickness of the cylinder in the impact region (time*10^{-6} s).

The impact region is defined by the radius of the sphere, and in this example the impact region is modeled by 5×5, 10×10, and 15×15 elements in the xy plane. The 15×15 impact region mesh refinement had a computer program execution of approximately 5000 s on the Cray XMP/48. The contact force vs time curves in Fig. 6 for the different impact region mesh refinements are very similar, with the 5×5 mesh refinement being the most conservative estimate for failure in an element.

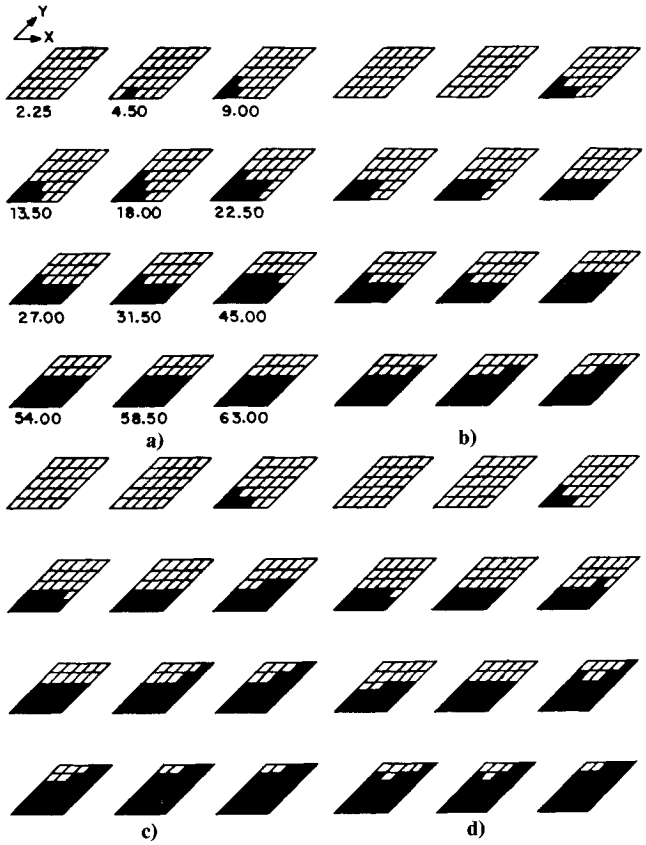

Fig. 8 Failure propagation in the outer negative: a) outer positive, b) inner negative, c) inner positive, and d) plies in the impact region of the composite cylinder (time*10^{-6} s).

The failure propagation for specific time intervals in the 5×5 mesh refinement of the impact region is presented in Figs. 7 and 8. The thickness of the composite cylinder is exaggerated to the membrane length, so that failure propagation can be easily seen. Initially, the failure propagation starts in the outer hoop plies and extends into the inner polar layers. As the duration of the contact force increases, the failure propagates along the outer hoop ply fibers, along the top negative inner polar layer fibers, and along the positive-negative-positive polar layer fibers in the positive polar layer fiber direction. The latter phenomena might be a result of the cylindrical response to the spherical impact and the geometry of the cylinder.

Further examination of the Tsai-Wu failure criteria showed that the failure propagation can be attributed to both the normal stresses in the transverse direction and the shear stresses being dominant. This phenomenon could lead to both matrix cracking and delamination in the composite cylinder which Lloyd and Knight[30] had observed in their experimental results.

VII. Concluding Remarks

A mixed finite-element method has been presented which can be used in examination of the failure propagation in the impact region of the composite cylinder subjected to low-velocity impact. The results obtained with the two-dimensional clamped and simply supported plate problems compared well with the results given by other methods. In extending this method to three dimensions, a failure criterion was used to analyze the failure propagation in the impact region of the composite cylinder due to a low-velocity impact. The results showed that the failure propagated from the outer-hoop ply fibers and into the inner-hoop polar layers. As the duration of contact increased, the inner polar layers failed, and the failure propagated from the inward polar layers to the outer hoop layers. Further study could include the degrading of the matrix

moduli and the modeling of the delamination modes so that a real-time computational model might be achieved.

Acknowledgment

Dr. Bachrach wishes to acknowledge the computational support from the Pittsburgh Supercomputing Center, PSCA Grant MSM-870030P.

References

[1]Pian, T. H. H., "Derivation of Element Stiffness Matrices by Assumed Stress Distributions," *AIAA Journal,* Vol. 2, July 1964, pp. 1333-1336.

[2]Herrmann, L. R., "Elasticity Equations for Nearly Incompressible Materials by a Variational Theorem," *AIAA Journal,* Vol. 3, Oct. 1965 pp. 1896-1900.

[3]Mandell, J. F., Wang, S. S., and McCarry, F. J., "Fracture of Graphite Fiber Reinforced Composites," Wright-Patterson AFB, OH, Air Force Materials Lab., AFML-TR-74-167, June 1974.

[4]Wang, S. S. Mandell, J. F., and McCarry, F. J., "A Multilayer Hybrid-Stress Fnite Element Analysis of a Through-Thickness Edge Crack in a 45° Laminate," *Engineering Fracture Mechanics,* Vol. 9, No. 1, 1977, pp. 217-238.

[5]Pian, T. H. H. and Sumihara, K., "Rational Approach for Assumed Stress Finite Elements," *International Journal for Numerical Methods in Engineering,* Vol. 20, Sept. 1984, pp. 1685-1695.

[6]Belytschko, T. and Bachrach, W. E., "Efficient Implementation of Quadrilaterals with High Coarse-Mesh Accuracy," *Computer Methods in Applied Mechanics and Engineering,* Vol. 54, 1986, pp. 279-303.

[7]Bachrach, W. E., "An Efficient Formulation of Hexahedral Elements with High Accuracy for Bending and Incompressibility," *Computers and Structures,* Vol. 26, No. 3, 1987, pp. 453-468.

[8]Sun, C. T. and Huang, S. N., "Transverse Impact Problems by Higher Order Beam Finite Elements," *Computer and Structures,* Vol. 5, Nos. 5-6, 1975, pp. 297-303.

[9]Sun. C. T. "An Analytical Method for Evaluation of Impact Damage Energy of Laminated Composites," *Composite Materials: Testing and Design, Fourth Conference,* ASTM STP 617, 1977, pp. 427-442.

[10]Tan, T. M. and Sun, C. T., "Use of Statical Indentation Laws is the Impact Analysis of Laminated Composite Plates," *Transactions of the ASME: Journal of Applied Mechanics,* Vol. 107, 1985, pp. 6-12.

[11]Wu, H.-Y. T. and Chang, F.-K., "Transient Dynamic Analysis of Laminated Composite Plates Subjected to Transverse Impact," *Computers and Structures* (to be published).

[12]Wu, H.-Y. T. and Springer, G. S., "Impact Induced Stress, Strains, and Delaminations in Composite Plates," *Journal of Composite Materials,* Vol. 22, June 1988, pp. 533-560.

[13]Wu, H.-Y. T. and Springer, G. S., "Measurements of Matrx Cracking and Delamination Caused by Impact on Composite Plates," *Journal of Composite Materials,* Vol. 22, June 1988, pp. 518-532.

[14]Lee, J. D., "Three-Dimensional Finite Element Analysis of Layered Fiber-Reinforced Composite Materials," *Computers and Structures,* Vol. 12, No. 3, 1980, pp. 319-339.

[15]Lee, J. D., "Three-Dimensional Finite Element Analysis of Damage Accumulation in Composite Laminates," *Computers and Structures,* Vol. 15, No. 3, 1982, pp. 335-350.

[16]Lee, J. D., Du, S., and Liebowitz, H., "Three-Dimensional Finite Element and Dynamic Analysis of Composite Laminate Subjected to Impact," *Computers and Structures,* Vol. 19, Nos. 5-6, 1984, pp. 807-813.

[17]Pian, T. H. H., Chen, D. P., and Kang, D., "A New Formulation of Hybrid/Mixed Finite Elements," *Computers and Structures,* Vol. 16, Nos. 1-4, 1983, pp. 81-87.

[18]Bachrach, W. E., Liu, W. K., and Uras, R. A., "A Consolidation of Various Approaches in Developing Naturally Based Quadrilaterals," *Computer Methods in Applied Mechanics and Engineering,* Vol. 55, 1986, pp. 43-62.

[19]Belytschko, T. and Engelmann, B. E., "On Flexurally Superconvergent Four-Node Quadrilaterals," *Computers and Structures,* Vol. 25, No. 6, 1987, pp. 909-918.

[20]Flanagan, D. P. and Belytschko, T., "A Uniform Strain Hexahedron and Quadrilateral with Orthogonal Hourglass Control," *International Journal for Numerical Methods in Engineering,* Vol. 17, May 1981, pp. 679-706.

[21]Belytschko, T., Ong, J. S.-J., Liu, W. K., and Kennedy, J. M., "Hourglass Control in Linear and Nonlinear Problems," *Computer Methods in Applied Mechanics and Engineering,* Vol. 43, 1984, pp. 251-276.

[22]Goldsmith, W. E., *Impact: The Theory and Physical Behaviour of Colliding Solids,* Arnold, London, 1960.

[23]Bathé, K. J. and Wilson, E. L., *Numerical Methods in Finite Element Analysis,* Prentice-Hall, Englewood Cliffs, NJ, 1976, pp. 319-326.

[24]Hashin, Z., "Failure Criteria for Unidirectional Fiber Composites," *Transactions of the ASME: Journal of Applied Mechanics,* Vol. 47, June 1980, pp. 329-334.

[25]Hashin, Z., "Analysis of Composite Materials—A Survey," *Transactions of the ASME: Journal of Applied Mechanics,* Vol. 50, Sept. 1983, pp. 481-505.

[26]Reddy, J. N. and Pandey, A. K., "A First Ply Failure Analysis of Composite Laminates," *Computers and Structures,* Vol. 25, No. 3, 1987, pp. 371-393.

[27]Karas, K., "Platten Unter Seitlichem Stoss," *Ingenieur Archiv,* Vol. 10, 1939, pp. 237-250.

[28]Chen, J. K. and Sun, C. T., "On the Impact of Initially Stressed Composite Laminates," *Journal of Composite Materials,* Vol. 19, Nov. 1985, pp. 490-504.

[29]Wu, H.-Y. T. "Impact Damage of Composites," Ph.D. Dissertation, Stanford Univ., Palo Alto, CA, 1986.

[30]Lloyd, B. E. and Knight, K. N., "Impact Damage Sensitivity of Filament-Wound Composite Pressure Vessels," Morton Thiokol Inc./Wasatch Operations, Brigham City, UT.